Long term X-ray spectral variability of the nucleus of M 81

V. La Parola[1,2], G. Fabbiano[2], M. Elvis[2], F. Nicastro[2], D.W. Kim[2], G. Peres[1]

[1] *Dipartimento di Scienze Fisiche ed Astronomiche, Sezione di Astronomia, Piazza del Parlamento 1, 90134 Palermo, Italy;*

[3] *Harvard Smithsonian Center for Astrophysics, 60 Garden St., 02138 Cambridge, MA*

ABSTRACT

We have analysed the soft X-ray emission from the nuclear source of the nearby spiral galaxy M 81, using the available data collected with ROSAT, ASCA, BeppoSAX and *Chandra* . The source flux is highly variable, showing (sometimes dramatic: a factor of 4 in 20 days) variability at different timescales, from 2 days to 4 years, and in particular a steady increase of the flux by a factor of $\gtrsim 2$ over 4 years, broken by rapid flares. After accounting for the extended component resolved by *Chandra* , the nuclear soft X-ray spectrum (from ROSAT/PSPC, BeppoSAX/LECS and *Chandra* data) cannot be fitted well with a single absorbed power-law model. Acceptable fits are obtained adding an extra component, either a multi-color black body (MCBB) or an absorption feature. In the MCBB case the inner accretion disk would be far smaller than the Schwartzchild radius for the $3-60\times10^6 M_\odot$ nucleus requiring a strictly edge-on inclination of the disk, even if the nucleus is a rotating Kerr black hole. The temperature is 0.27 keV, larger than expected from the accretion disk of a Schwartzchild black hole, but consistent with that expected from a Kerr black hole. In the power-law + absorption feature model we have either high velocity (0.3 c) infalling CV clouds or neutral CI absorption at rest. In both cases the C:O overabundance is a factor of 10.

Subject headings: X-rays: galaxies — galaxies: nuclei — galaxies: individual (M81)

1. INTRODUCTION

M81 (NGC 3031) is a nearby galaxy (3.6 Mpc, Freedman et al. 1994), with well defined spiral arms and a prominent bulge, with a structure similar to that of M31. Its nucleus is the

[2]e-mail: laparola@oapa.astropa.unipa.it

nearest example of a low luminosity AGN (Peimbert & Torres-Peimbert 1981; Elvis & van Speybroeck 1982) and has been studied at all frequencies; its emission properties make it both a LINER (Low Ionization Nuclear Emission line Region; Ho, Filippenko, Sargent 1996) and a LLAGN (Low Luminosity AGN): it contains a broad component of the $H\alpha$ emission line (Peimbert & Torres-Peimbert 1981), a compact radio core (Bietenholz et al. 1996) and a variable point-like X-ray source ($L_X \sim 10^{40}$ erg/s), M81 X-5 (Elvis & van Speybroeck 1982; Fabbiano 1988) with a power law continuum with photon index $\Gamma \sim 1.85$ in the 2-10 keV energy band (Ishisaki et al. 1996; Pellegrini et al. 2000). Broad line velocity (Ho, Filippenko, Sargent 1996) and stellar dynamics (Bower et al. 2000) studies suggests a super-massive black hole of $3 \times 10^6 M_\odot < M_{BH} < 6 \times 10^7 M_\odot$.

ASCA (0.5-10.0 keV, Ishisaki et al. 1996) and BeppoSAX (0.1-100 keV, Pellegrini et al. 2000) spectral analyses of the nuclear X-ray source show, in addition to the power-law component ($\Gamma \sim 1.85$), a 6.7 keV He-like Fe resonance line and a thermal component with $kT \sim 0.86$ keV (Ishisaki et al. 1996). A more recent study by Immler & Wang (2001), which uses all the co-added available PSPC observations and fixes the power-law photon index to the ASCA/BeppoSAX $\Gamma = 1.85$ confirms this soft component and models it with a two-temperature optically thin plasma, ascribing it to the presence of optically thin diffuse gas (kT=0.15 keV) and to a population of X-ray binaries and SNR (kT=0.63 keV). However this type of source would be harder than 0.63 keV.

Significant variability in the flux of the nuclear X-ray source on a short timescale ($\sim$ 600 s) was reported by Barr et al (1985) using EXOSAT data. Longer timescale ($\sim$ 2 days to few years) variability has also been reported (Pellegrini et al. 2000; Ishisaki et al. 1996; Immler & Wang 2001). No spectral variability has been reported; however, a full study of the spectral behaviour using the wealth of data collected from the nucleus of M81 has not been done so far. In the present paper we revisit the soft X-ray emission of the nucleus of M81 through the observations of ROSAT instruments concentrating on variability, and compare these data with those from ASCA, BeppoSAX and *Chandra* . In particular, the ROSAT/PSPC data give us the opportunity to study any spectral variation of soft X-ray emission that occurred during the extensive ROSAT coverage of M81. This paper is structured as follows: Section 2 illustrates the data and their reduction; in Section 3 we describe the source variability; Section 4 is devoted to spectral analysis; our results are discussed in Section 5.

2. OBSERVATIONS AND DATA REDUCTION

A log of all the observations of M81 is given in Table 1. M81 was observed 22 times with ROSAT in a period of seven years from 1991 to 1998: 12 times with the PSPC (Position Sensitive Proportional Counter; Pfeffermann et al. 1987) and 10 times with the HRI (High Resolution Imager; David et al. 1996). This frequent coverage is mainly due to the monitoring of the supernova SN1993J (Zimmermann et al. 1994), 2.7' south of the nucleus of M81, whose evolution was followed with roughly one observation every six months. The large field of view of the PSPC (2° diameter) and of the HRI (30' diameter) ensures that the nucleus is included in every observation of SN1993J. The data have been processed using the IRAF(v. 2.11)/PROS (v. 2.5) software system (Tody 1986; Worrall et al. 1992).

The radius for source photon selection for the PSPC depends on the position of the source on the detector plane, because the radius of the Point Spread Function (PSF) increases with the distance from the center of the field of view (FOV) (Boese 2000); for the on-axis observations we used a source radius of 3', which includes 95% of the emission at all energies and an annular background region with inner and outer radii 3' and 7' respectively. For the off-axis observations the source position and radius were evaluated with the GALPIPE processing (Damiani et al 1997) applied to each observation and from the ROSAT/PSPC point spread function description (Boese 2000): the radius is 5' and 6', for M81 nucleus off-axis positions of 16' and 36' to 42', respectively. We have excluded any part of the selected region obscured by the PSPC window supporting ribs. The background was extracted from an annular region with outer and inner radii 12' and 6' respectively, after subtraction of the contribution of point sources. For convenience of reference, we designate the PSPC pointings P1-P12 in time order.

The ten HRI observations pointed on M81 (H1-H10) have a total exposure time of 177 ksec. For each observation we used the position of the detected sources[2], excluding the nuclear source M81 X-5, to check for possible misalignements of the astrometric frames and to correct for small spacecraft errors; no further alignment was needed. The PSPC and HRI position determinations are consistent with each other and from now on we will use the more accurate HRI centroid coordinates: RA $9^h57^m54.3 \pm 0.1^s$ and Dec $69°03'46.4 \pm 0.5$" (J2000). For each HRI observation, source counts were extracted from a circular region with 1.3' radius, as found with the LDETECT IRAF/PROS algorithm (S. Dyson 1999, private communication).

The 21 available ASCA observations of M81 (A1-A21) were also used to estimate the

[2]using the detection algorithm in the IRAF/PROS task XEXAMINE

flux of the nucleus (see Table 1; for a detailed analysis of these data see Ishisaki et al. 1996 and Iyomoto & Makishima 2001). The ASCA/SIS data are less contaminated by the SN1993J emission than the ASCA/GIS ones. We extracted ASCA/SIS spectra from a 4' circular region centered on the apparent centroid of the M81 X-5 emission, excluding a 2' circular region centered on the supernova (that lies 2.8' from M81 X-5). The background was extracted from the portion of the SIS chip not contained in the above regions.

BeppoSAX observed M81 on June 4 1998. This observation was studied in detail by Pellegrini et al. (2000). Here, we compare the SAX/LECS (Low Energy Concentrator Spectrometer) spectrum and ROSAT/PSPC spectra in order to check for spectral variability. For the BeppoSAX data, we used the standard source and background spectra provided by the Narrow Field Instruments public archive[3], extracted from a 6' radius region centered on the source centroid position.

Chandra /ACIS has observed M81 twice (Ho et al. 2001, Swartz et al. 2003). We used the observation with the longest exposure time (50 ksec, Table 1) . The high flux of the nucleus produces $> 80\%$ of pile-up fraction, making the direct study of the properties of the nucleus unreliable. We therefore used the read-out trailed image of the nucleus to extract a spectrum unaffected by pile-up, using a narrow box region (5") running along the read-out direction of the chip containing the nuclear trailed image and excluding the direct image. The background was extracted from two similar regions adjacent to the source region, each 5" wide. In the following, this spectrum will be referred to as *Chandra* -T. The sub-arcsecond *Chandra* PSF allows the study of the circum-nuclear region, and in particular of its contribution to the ROSAT and BeppoSAX spectra. To this aim we extracted separately the spectra of the point-like sources (spectrum **a**) and of the unresolved emission (spectrum **b**), using the same extraction radius as for the on-axis ROSAT spectra (3'). The coordinates of the point-like sources are from Swartz et al. (2003). We excluded the point-like nuclear source (a circular region with a 10" radius) and the read-out trailed image (from a strip 5" wide running along through the chip read-out direction). The background is extracted from the remaining portion of the chip.

[3]Available at http://www.asdc.asi.it/bepposax/

Table 1. Log of X-ray observations of M81.

Ref.[a]	Obs. id.	Live Time	Start Date	Angle[b]	Ref.[a]	Obs. id.	Live Time	Start Date	Angle[b]
1P	rp600101a00	9296	25/03/91	0.3'	1A	15000000	6480	05/04/93	2.9'
2P	rp600110a00	12717	27/03/91	36.9'	2A	15000120	30144	05/04/93	2.9'
3P	rp600052n00	6588	18/04/91	41.7'	3A	15000010	6622	07/04/93	10.1'
4P	rp600110a01	12238	15/10/91	36.9'	4A	15000130	35680	07/04/93	6.7'
5P	rp600101a01	11085	16/10/91	0.3'	5A	15000030	154847	16/04/93	6.6'
6P	rp600382n00	27120	29/09/92	0.3'	6A	15000020	29440	25/04/93	6.5'
7P	rp180015n00	17938	03/04/93	0.3'	7A	15000040	28576	01/05/93	6.6'
8P	rp180015a01	8731	04/05/93	2.8'	8A	15000050	85376	18/05/93	5.9'
9P	wp600576n00	16412	29/09/93	16.0'	9A	10018000	45152	24/10/93	4.0'
10P	rp180035n00	17800	01/11/93	0.3'	10A	51005000	80016	01/04/94	6.6'
11P	rp180035a01	4234	07/11/93	0.3'	11A	52009000	98206	21/10/94	7.5'
12P	rp180050n00	1849	31/03/94	0.3'	12A	53008000	24128	01/04/95	7.2'
1H	rh600247n00	26320	23/10/92	0.3'	13A	53008010	101434	24/10/95	7.6'
2H	rh600247a01	21071	17/04/93	0.3'	14A	54008000	103616	16/04/96	7.0'
3H	rh600739n00	19902	19/10/94	0.3'	15A	54008010	39712	27/10/96	7.7'
4H	rh600740n00	18984	13/04/95	0.3'	16A	55018000	100640	08/05/97	6.5'
5H	rh600881n00	14826	12/10/95	0.3'	17A	56020000	102672	10/04/98	6.9'
6H	rh600882n00	18328	15/04/96	0.3'	18A	56020010	98224	20/10/98	7.6'
7H	rh600882a01	5091	27/10/96	0.3'	19A	57048000	79794	06/04/99	7.4'
8H	rh601001n00	19231	29/03/97	0.3'	20A	57006000	97104	10/04/99	6.7'
9H	rh601002n00	12590	30/09/97	0.3'	21A	57006010	99808	20/10/99	7.6'
10H	rh601095n00	12590	25/03/98	0.3'	1S	40732001	100000	04/06/98	0.0'
					Ch	735	50570	07/05/00	2.8'

[a]Reference number for each observation. Instrumests are coded as: P=ROSAT/PSPC; H=ROSAT/HRI; A=ASCA; S=SAX; Ch=*Chandra*

[b]Nominal off-axis angle of the optical center of M81 on the detector

3. ROSAT TEMPORAL ANALYSIS

The ROSAT data form a long series of uniform observations, suitable for temporal analysis. Instead, the wide beam of ASCA and BeppoSAX data includes much galaxian emission, and we do not include them in the following analysis, except for the long-term light-curve. In Figure 1 we show the 1991-1999 long term light curve of the nucleus of M81 in the 0.5-2.4 keV band. The PSPC fluxes were calculated assuming a power-law with $\Gamma = 1.79$ plus a thermal component with $kT \sim 0.5$ keV, obtained as final result of the spectral analysis (see Section 4). The same model was used to calculate the fluxes from the ROSAT/HRI count rates, through the PIMMS tool[4]. ASCA/SIS fluxes were evaluated using a power-law model, since the soft thermal component is negligible in the ASCA spectral band; the BeppoSAX flux was extrapolated from the value reported in Pellegrini et al. (2000) for the 0.1-2.0 keV band using their best-fit model. We note that the light curve in Figure 1 has been derived using data from four different detectors, and therefore one may expect some cross-calibration problems. In our case this is not a problem, since data taken with different instruments very close in time give consistent results. This happens in most HRI/ASCA pairs of data (see, for example, the groups of observations at $5.00 \times 10^4 d$, $5.02 \times 10^4 d$, $5.04 \times 10^4 d$); see also the group of observation at $5.09 \times 10^4 d$ which consists of HRI, ASCA and BeppoSAX points.

We observe a factor of 2-4 flux difference between the two high count-rate PSPC observations 1P and 3P and all the other PSPC pointings (all of which yield a similar, lower, count rates). We can confidently exclude an unlikely variability in the instrumental calibration, because no flux enhancement is seen in any of the sources in the field (see, e.g., X-9 La Parola et al. 2001 and other fainter sources (Immler & Wang 2001). We can also rule out transient sources near the nucleus, because there is no significant spectral variation between 1P and 3P and the immediately following pointings (Section 4). The above considerations suggest that this variation should be ascribed entirely to the nuclear source.

To search for short term variations, we examined the light-curves from individual ROSAT observations. Figure 2 presents these light-curves in order of their observation. Each bin corresponds to one GTI (Good Time Interval [5]) and the time is given in days starting from the ROSAT launch (June 1990).

---

[4]Portable Interactive Multi-Mission Simulator, at http://asc.harvard.edu/toolkit/pimms.jsp

[5]Most targets are occulted by Earth for part of the orbit and the observations are broken into smaller segments which may be interleaved with observations of other targets. Hence, the resulting data stream for a particular target will in general show large data gaps, with effective observing intervals lasting a few hundreds of seconds; each of these continuous observation is a "Good Time Interval".

The data show variability on three different timescales:

• Slow variability: a slow regular ascending trend can be observed, starting on November 1993 and ending on April 1996, with a difference of a factor of ~ 2 in the flux between the first and the last point (Figure 1). This trend was reported by Pellegrini et al. (2000) and Iyomoto & Makishima (2001) for the 2.0-10.0 keV band from BeppoSAX and ASCA data.

• Medium variability: both before and after the period of regularly increasing flux, there are two periods of irregular variability (Figure 1). This is more marked before November 1993, where two very bright flare-like episodes are seen, with variations up to 4 times in flux. It is weaker (but nevertheless extremely significant) after April 1996. This kind of variability was not previously reported.

• Fast variability: the lightcurves of many observations (Figure 2) show variability of up to 30% on timescales of the order of one day (e.g. observations 9P, 4H, 6H, 9H), as found with BeppoSAX (Pellegrini et al. 2000), or even a few hours (e.g. observations 5P, 9P, 10H), confirming the early EXOSAT report (Barr et al 1985).

A Kolmogorov-Smirnov variability test (KS, see, e.g., Conover 1971) applied to the unbinned data and a χ^2 test applied to the light curves binned into GTI show that 11 out of 22 observations are variable in both tests with more than 99% probability of rejecting the hypothesis of constant rate (Table 2). Despite the abrupt drop in flux by a factor of ~ 3 in one day between observations 1P and 2P and the factor of ~ 2 rise 20 days later between 2P and 3P (Figures 1 and 2), the individual light curves of these observations do not show any sharp change of the count rate.

We investigated the spectral variability in the PSPC observations by calculating a hardness ratio of each observation in two pairs of bands (Table 2). The first, HR1: 0.11-0.42 keV/ 0.52-2.02 keV, covers the whole spectral range of the PSPC and can give information on the absorbing column. The second HR2: 0.52-0.91 keV/ 0.92-2.02 keV, covers only the hardest part of the spectrum and is more sensitive to spectral index variations. We performed a χ^2 test against the ipothesis of constant distribution centered on the average value: HR1 does not show any variability ($\chi^2/\nu = 13.6/11$, where ν is the number of degrees of freedom) while HR2 shows evidence of variability ($\chi^2/\nu = 65/11$). We found no evidence of correlation of the hardness ratio with the total flux (Figure 3). The spectral analysis revealed that the spectrum is indeed variable, as discussed in Section 4.

Table 2. Properties of individual ROSAT observation of M81.

Ref.	Γ[a]	Flux[b]	P_{KS}[c]	P_{χ^2}[d]	HR1[e]	HR2[e]
1P	2.20 ± 0.08	15.12	0.21	0.26	0.765 ± 0.011	0.227 ± 0.007
2P	1.92 ± 0.15	7.67	< 0.01	< 0.01	0.773 ± 0.018	0.237 ± 0.012
3P	2.10 ± 0.12	19.37	0.49	0.01	0.755 ± 0.015	0.201 ± 0.010
4P	2.1 ± 0.2	4.51	< 0.01	< 0.01	0.832 ± 0.026	0.220 ± 0.016
5P	2.22 ± 0.10	7.34	0.16	< 0.01	0.751 ± 0.014	0.229 ± 0.010
6P	2.30 ± 0.07	7.41	< 0.01	< 0.01	0.755 ± 0.009	0.196 ± 0.006
1H	···	6.29	< 0.01	< 0.01	···	···
7P	2.32 ± 0.09	6.94	< 0.01	< 0.01	0.756 ± 0.011	0.186 ± 0.008
2H	···	7.22	0.53	0.71	···	···
8P	2.25 ± 0.12	7.37	< 0.01	< 0.01	0.757 ± 0.016	0.195 ± 0.011
9P	2.18 ± 0.10	6.67	< 0.01	< 0.01	0.785 ± 0.014	0.234 ± 0.009
10P	2.41 ± 0.06	9.00	0.55	0.50	0.751 ± 0.010	0.177 ± 0.007
11P	2.47 ± 0.20	6.71	0.02	0.03	0.749 ± 0.023	0.162 ± 0.016
12P	$2.2^{+0.4}_{-0.3}$	6.91	0.06	0.14	0.768 ± 0.037	0.224 ± 0.025
3H	···	9.64	0.16	0.40	···	···
4H	···	9.81	< 0.01	< 0.01	···	···
5H	···	11.32	< 0.01	< 0.01	···	···
6H	···	13.79	< 0.01	< 0.01	···	···
7H	···	12.46	< 0.01	< 0.01	···	···
8H	···	8.34	0.02	0.03	···	···
9H	···	12.02	< 0.01	< 0.01	···	···
10H	···	16.56	< 0.01	0.09	···	···

[a]Best fit power-law photon index

[b]Average flux in units of 10^{-12} erg s^{-1} cm^{-2}. The model used to calculate fluxes are described in Section 3.

[c]Probability of a constant count rate within the observation according to a Kolmogorof-Smirnof test

[d]Probability of a constant count rate equal to the average count rate according to a χ^2 test

[e]Average PSPC hardness ratios defined as $HR = \frac{H-S}{H+S}$, where $H_{HR1} = C_{0.52-2.02}$, $S_{HR1} = C_{0.11-0.42}$, $H_{HR2} = C_{0.92-2.02}$, $S_{HR2} = C_{0.52-0.91}$ are the photon counts in the subscripted energy bands (in keV).

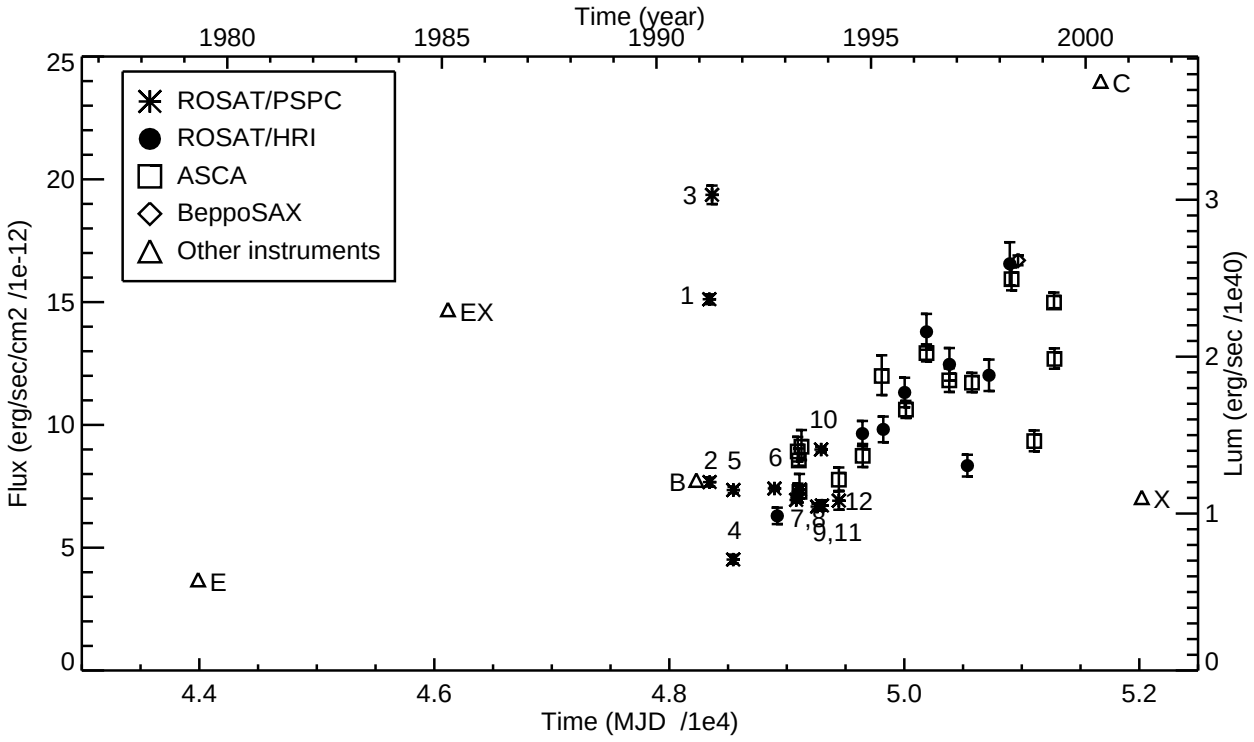

Fig. 1.— Observed flux (not corrected for cold absorption) in the 0.5-2.4 keV band (left Y axis). The details on models used for flux calculation and spectral analysis are given in Sections 3 and 4. The luminosity (right Y axis) is calculated assuming a distance of 3.6 Mpc (Freedman et al. 1994). The points from other instruments are derived from the literature and are marked as follows: E = *Einstein*/IPC (Fabbiano 1988); EX = EXOSAT and B = BBXRT (Petre et al. 1993); C = *Chandra* /ACIS (Swartz et al. 2003); X = XMM (Page et al. 2003) The numbers near the symbols of the twelve PSPC observations show the time sequence of the relevant data points and clarify the rapid and large transients in the first part of the light curve.

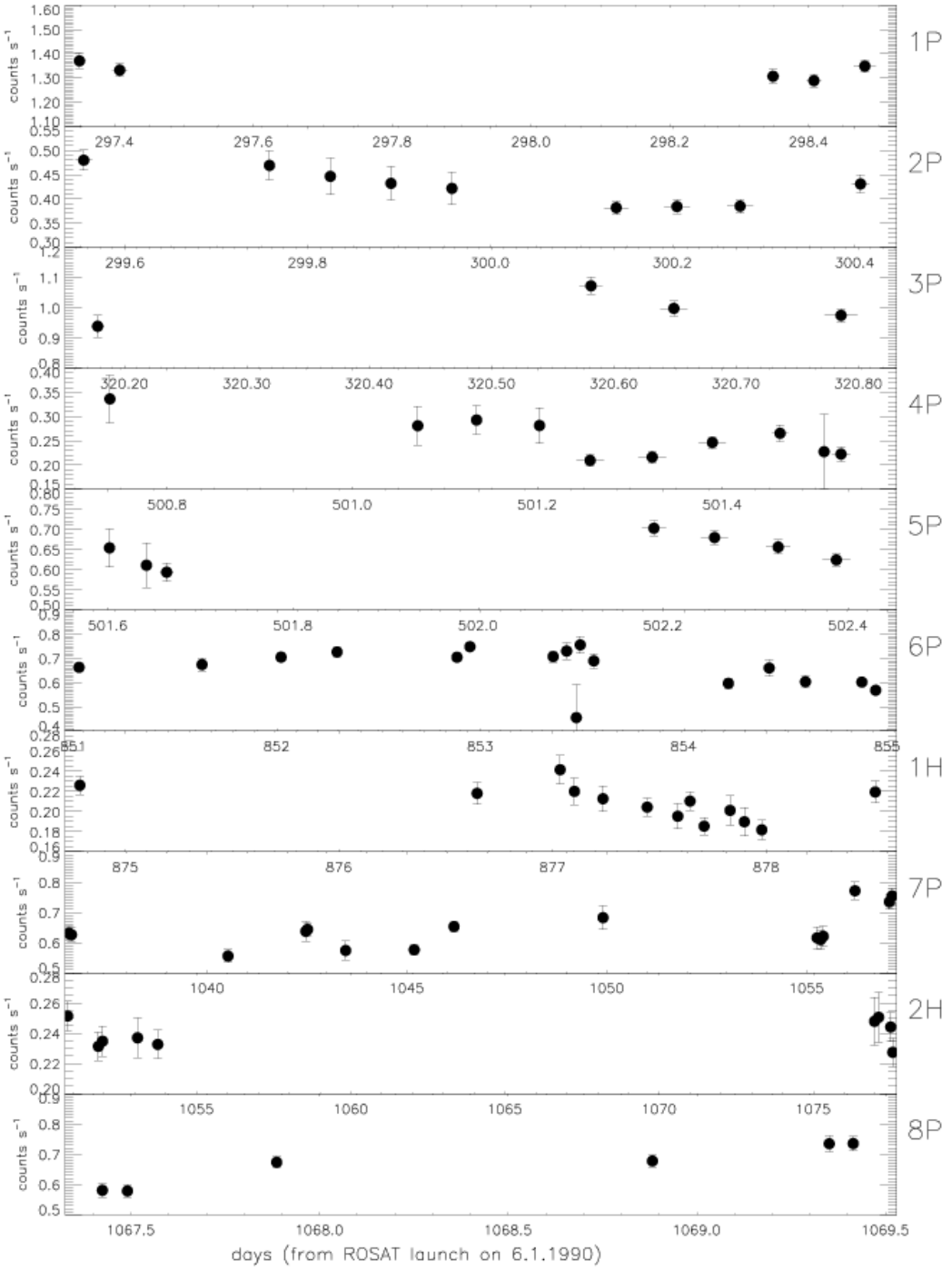

Fig. 2.— Light curves of PSPC and HRI observations (identified with a P and a H on the right of the graph respectively). Time is in days since the satellite launch (June 1990); the number on the right of each curve identifies the observations sequence as in Table 1.

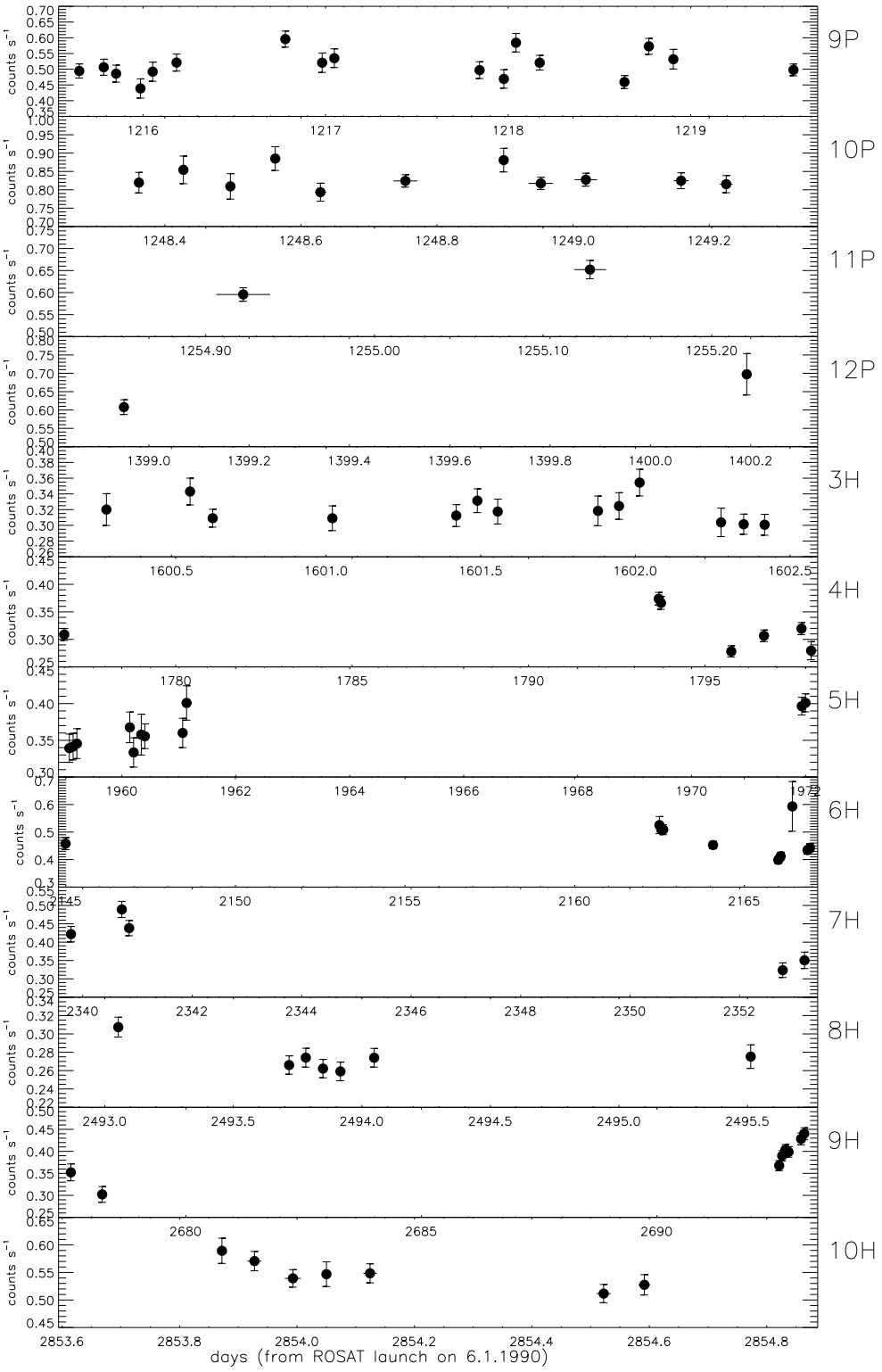

Fig. 2.— *Continued*

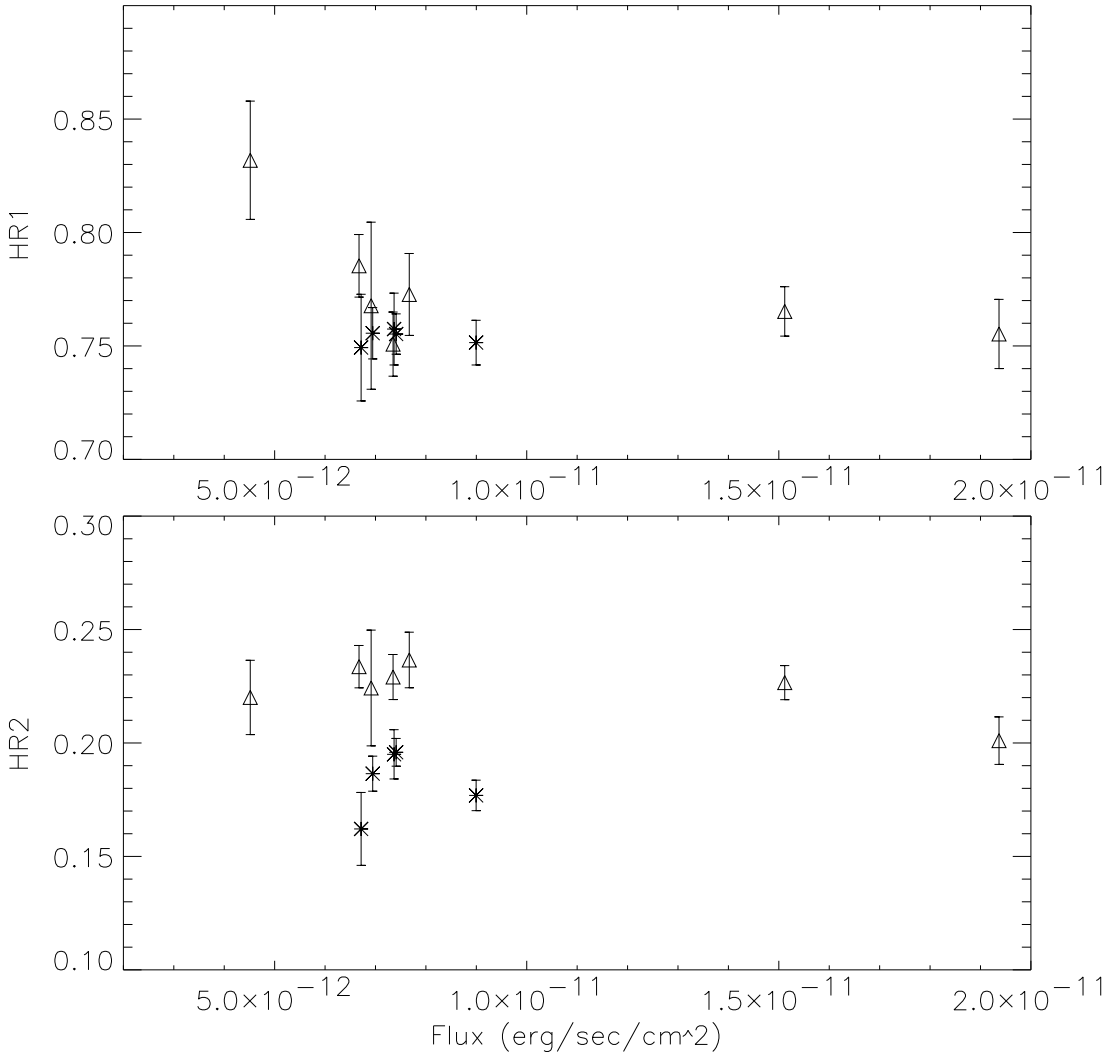

Fig. 3.— Hardness ratios (as defined in Table 2) vs. count rate. Triangles and stars indicate respectively the observations with and without the strong absorption feature (see Sections 4.2 for a discussion)

4. SPECTRAL ANALYSIS

The spectra were analysed using the software XSPECv 10.0/11.1 (Arnaud, George and Tennant 1992).

4.1. The galactic emission

The large beam spectra from BeppoSAX and ROSAT include a significant contribution from the circumnuclear region of the galaxy, within the 3' extraction radius around the nucleus. The high resolution *Chandra* observation allows us to measure the galaxy emission (both diffuse and from individual point sources) included in the wider beam ROSAT and BeppoSAX spectra. As described in Section 2, we used the same extraction radius as for the ROSAT data (3'), but excluded the region affected by the nuclear point source and the strip containing the trailed image of the nucleus. We then extracted two spectra: **a)** the individual point source spectrum, obtained summing the spectra of the bright sources falling within the 3' circle, as listed in Swartz et al. (2003), **b)** the diffuse spectrum, i.e. the emission within the same region excluding the point sources. These have roughly equal fluxes. We then formed the total spectrum **c)**, summing the diffuse and the point-source spectra. We fitted simultaneously the spectra **a)**, **b)** and **c)**, imposing the best fit model of spectrum **c)** to be the sum of the best fitting model of spectra **a)** and **b)**. The best fit parameters are in Table 3. We find that spectrum **a)** can be described with power-law with $\Gamma \sim 1.7$ plus a multicolor black body (MCBB, model DISKBB in XSPEC) at ~ 0.08 keV and a gaussian at ~ 0.8 keV. To describe spectrum **b)** we need a Raymond-Smith spectrum at ~ 0.25 keV and, again, a power-law with $\Gamma \sim 1.7$. Spectra **a)** and **b** are not consistent with each other. However, in both cases the NH is consistent with the Galactic line of sight value and the two power-law slopes are consistent with each other. In merging the models to fit spectrum **c** we used only a single power-law component. The [0.5-2.4] keV flux corrected for absorption by the best fit NH is 8.1×10^{-13} erg sec^{-1}cm^{-2} for the integrated point source emission and 6.9×10^{-13} erg sec^{-1}cm^{-2} for the diffuse emission, for a total of 1.5×10^{-12} erg sec^{-1}cm^{-2} .

4.2. The nuclear spectra

We first analysed the ROSAT spectra, extracted with the IRAF routine QPSPEC and processed with PROSCON, using the response matrices publicly available through the HEASARC/ROSAT

webpage[6]. As a preliminary step, we fitted the spectra of each of the 12 observations with a simple absorbed power law model, in order to search for spectral variability. A comparison of residuals of each observation to the relevant best fit model (Figure 4) shows that some observations (6P, 7P, 8P, 10P, hereafter "dip" observations) show a large dip in the residuals between 0.2 and 0.7 keV, while the remaining seven observations (hereafter "flat") are well described by a power-law.

We improved the statistics of the spectral fit by summing the spectra by type. We then fitted the two resulting spectra with a simple power-law. The results show that in the summed *dip* spectrum the absorption feature is clearly visible between 0.3 and 0.5 keV (Figure 5); however, in the summed *flat* spectrum there is also a broad, weak absorption-like structure, at the same energy, suggesting that the feature is in fact present in all the observations, albeit with varying intensity. We can confidently rule out the hypothesis that the feature is an instrumental effect, as there is no hint of it in the spectra of other sources of the same field (see e.g. X-9 in La Parola et al. 2001). In order to minimize the contribution from other bright sources in the vicinity of the nucleus, and because the effective area is poorly calibrated for off-axis PSPC sources, the subsequent analysis was carried on a spectrum selected from the sum of the eight observations where the nucleus was on-axis.

We also checked for the presence of the absorption feature in observations by other instrument. ASCA has too little response below 0.5 keV. We can however use SAX/LECS and *Chandra*-T (read-out trail) spectra (see Section 2 for details on the extraction of these spectra). We decided to fit the whole energy range (0.1-4.0 for LECS, 0.3-8.0 for ACIS, compared with 0.1-2.4 for PSPC), in order to have a better estimate of the continuum. We fitted each of these spectra with a simple power-law model (Table 4). An absorption feature at ~ 0.3 keV is seen in these spectra as well. This is made more evident in Figure 5, where we plot the residuals obtained by fitting with a power law only the energy range above 1.0 keV, that shows also how the feature is at slightly different energy in the three spectra.

We then made a more careful analysis (see Table 4) of the ROSAT/PSPC and SAX/LECS data by adding a fixed component to model the extended galaxy contribution, set to the best fit model derived from the *Chandra* data of the 3' radius extraction region around the nucleus (see Section 4.1) in addition to the variable components. A power-law plus this extended component gives a good fit to energies higher than 1 keV, but still overpredicts the emission between 0.3 and 0.6 keV. To investigate the nature of this "dip" we tested four models in which a single component was added to the power-law: an optically thin Raymond-Smith plasma, a multi-color black body accretion disk (MCBB), an absorption edge and a gaussian

[6]http://heasarc.gsfc.nasa.gov/docs/rosat/rosgof.html

line in absorption (Table 4). In all cases the improvement over a simple power-law model is highly significant, with F-test probabilities lower than 1%. The BeppoSAX and ROSAT data give similar results for both the MCBB and the Raymond-Smith components, with a better χ^2 for the disk model. In both cases, the edge model has a χ^2 comparable with that of the disk model. The energy of the edge found for BeppoSAX data ($0.22^{+0.03}_{-0.06}$ keV) is lower than for ROSAT data ($0.41^{+0.08}_{-0.13}$ keV). In the *Chandra* data we found that the fits require a lower temperature Raymond or MCBB component, while the edge energy is 0.29 ± 0.02 keV. The gaussian model significantly improves the fit of the *Chandra* data ($\chi^2/\nu = 104/127$) while for the PSPC data it is equivalent to the other models and for BeppoSAX it is slightly worse. The best fit energies of the gaussian absorption line are consistent with each other in the three instruments.

The power-law index in the ROSAT data is steeper than in the SAX data by $\Delta\Gamma \sim 0.4$ to 1.0, depending on the spectral model. An offset of $\Delta\Gamma \sim 0.4$ has been observed in other objects too (e.g. NGC5548 Iwasawa, Fabian & Nandra 1999), and is thought to be a systematic calibration offset. In this case the difference is sometimes larger than this offset (in NGC5548), suggesting that at least part of the steepening is real, and not an instrumental effect.
The luminosity of the power-law source in the 0.5-2.4 keV range is 2.3×10^{40}erg/s (corresponding to 1.6×10^{-11} erg sec^{-1}cm^{-2}) for BeppoSAX and 1.4×10^{40} erg/s (1.0×10^{-11} erg sec^{-1}cm^{-2}) for the PSPC data used in the spectral analysis. Since the contribution of circumnuclear emission from the *Chandra* analysis was included in the fit models for the ROSAT/PSPC and SAX/LECS data, these luminosities are truly representative of the nuclear source. The *Chandra*-T spectrum cannot be used directly to obtain a normalization, and thus a flux. We use here the estimate of Swartz et al. (2003), see Figure 1, which give $L_X = 3.8 \times 10^{40}$ erg/s in the 0.5-2.4 keV range (i.e. 2.6×10^{-11} erg sec^{-1}cm^{-2}).

In summary, our analysis revealed that the nuclear spectrum is consistent with a power-law plus a soft component that can be modelled either with an absorption feature at $0.3 \sim 0.4$ keV or with thermal disk emission (MCBB model) at $0.2 \sim 0.3$ keV. The spectrum is absorbed in excess of the Galactic NH, while the spectrum of the circumnuclear region (only from *Chandra* /ACIS data) does not show any excess absorption. The circumnuclear emission is modelled as two components, resolved point sources (described with a power-law plus a MCBB, with $L_X = 1.2 \times 10^{39}$ erg/s) and diffuse emission (described with a power-law plus a Raymond-Smith model, with $L_X = 1.0 \times 10^{39}$ erg/s), that contribute for a total of $L_X = 2.2 \times 10^{39}$ erg/s (i.e. 1.5×10^{-12} erg sec^{-1}cm^{-2}).

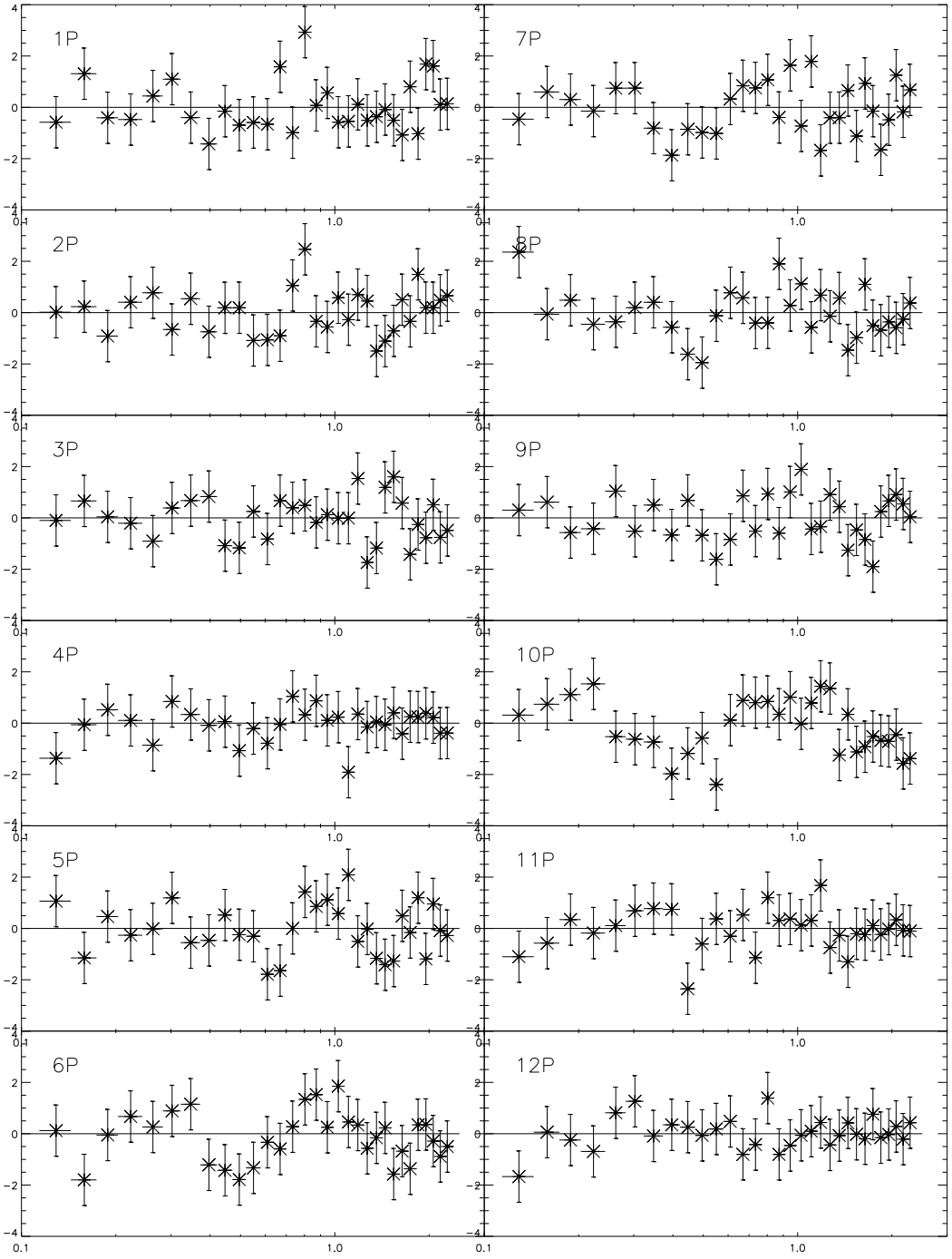

Fig. 4.— Residuals in units of χ for all the PSPC spectra best-fitted with a power law model

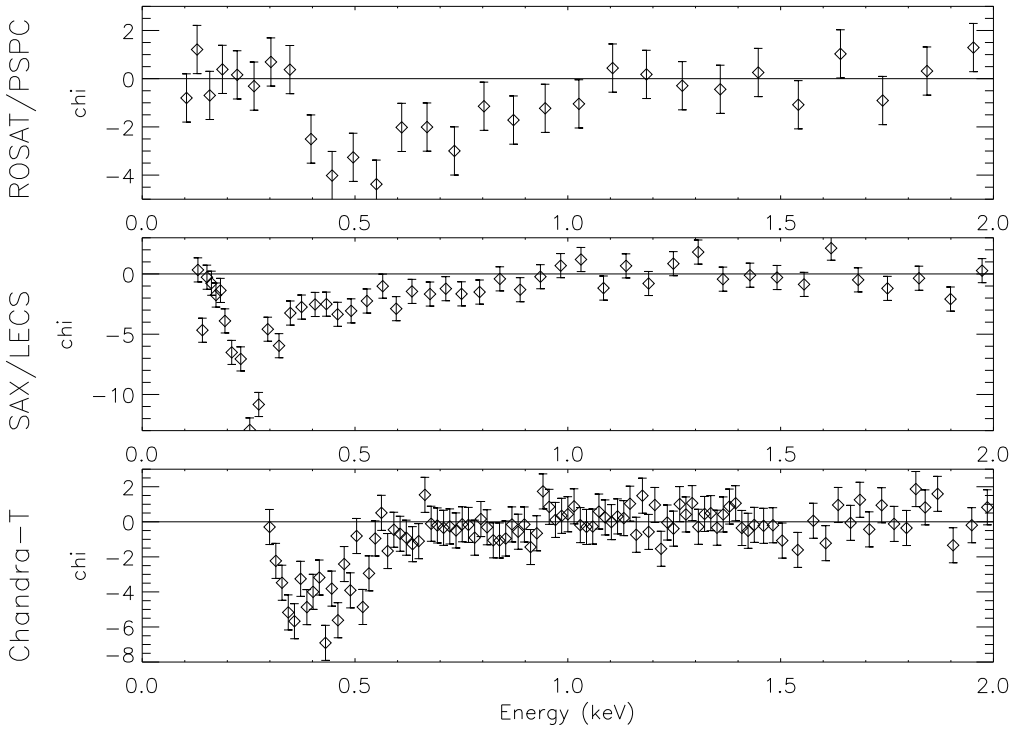

Fig. 5.— Spectra of the nucleus of M81: residuals with respect to a power-law model. Form top to bottom: ROSAT/PSPC spectrum (obtained from the sum of the on-axis observations), SAX/LEX spectrum, *Chandra* -T spectrum. These residuals have been obtained fitting with a power law energy range not affected by the absorption feature: 0.1-0.3 keV and 1.0-2.4 keV for the PSPC and > 1.0 keV for LECS and *Chandra* -T

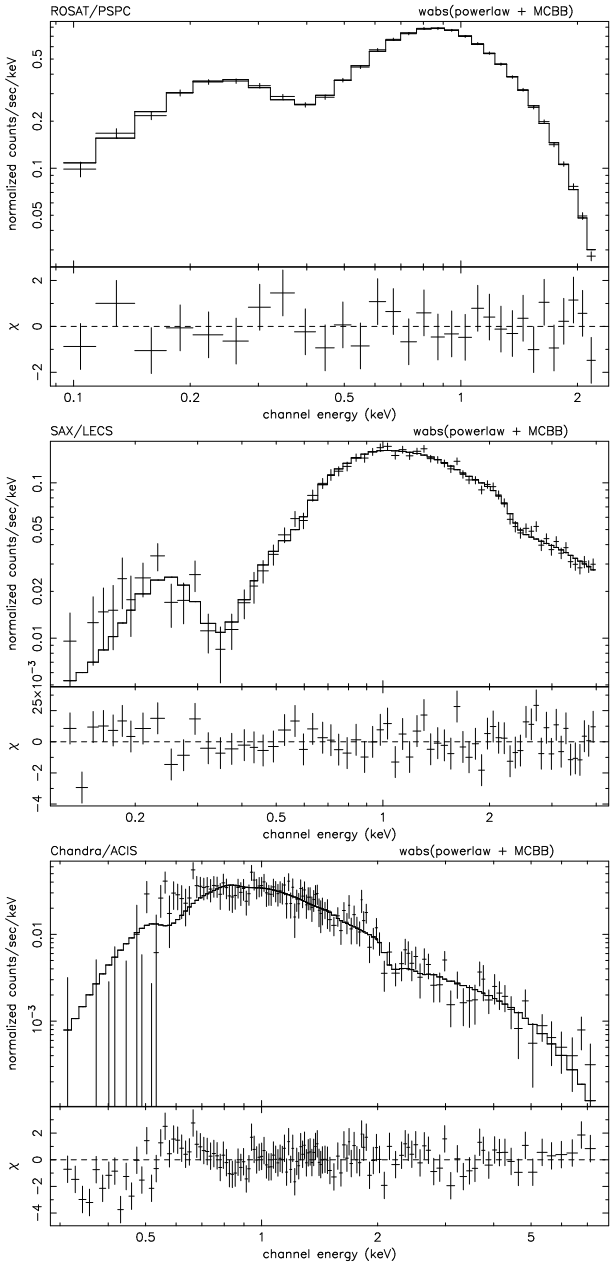

Fig. 6.— Spectra, best fit model and residuals of the nucleus of M81 for the MCBB. **Top**: PSPC; **Middle**: SAX/LECS; **Bottom**: *Chandra* -T

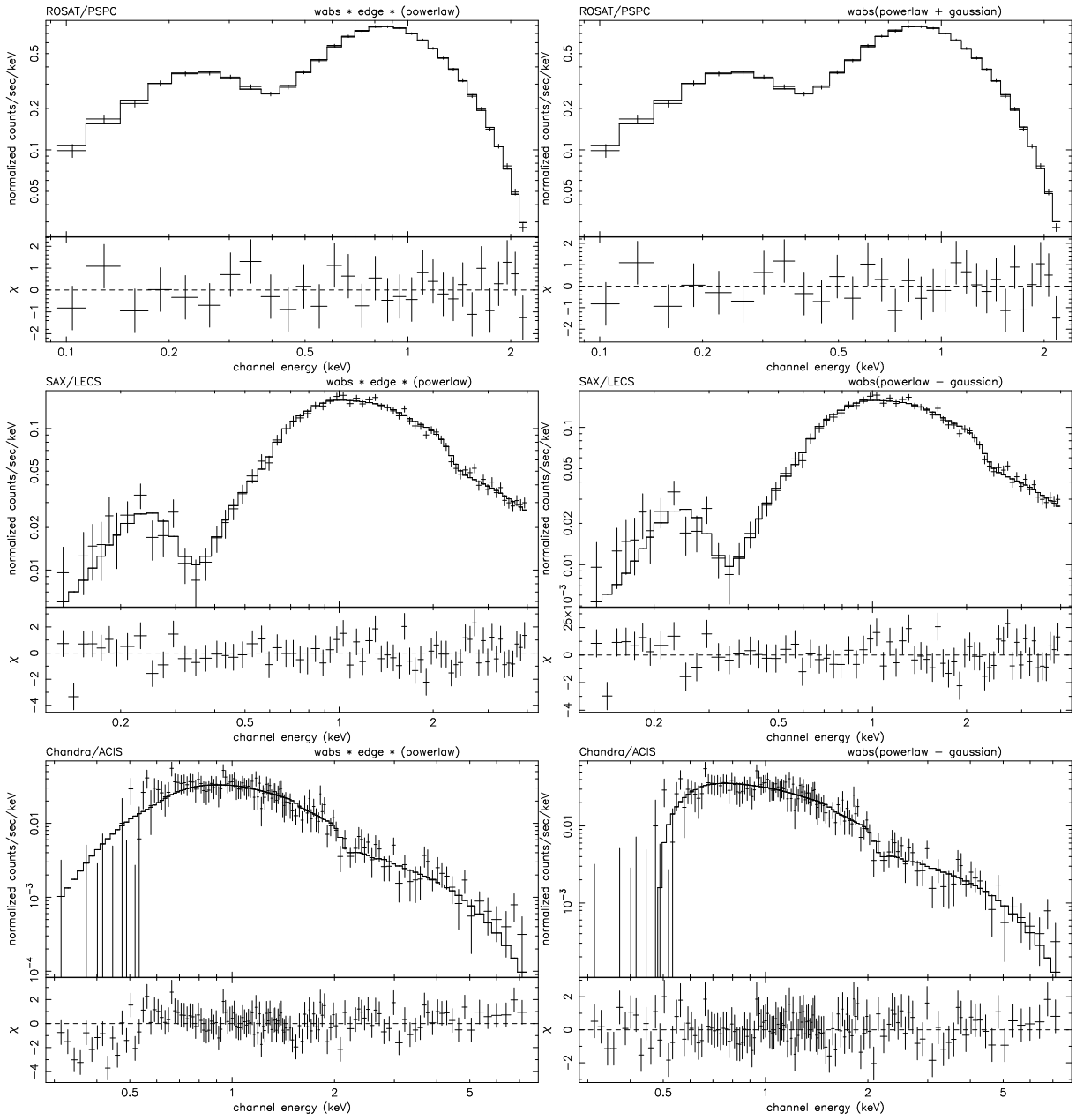

Fig. 7.— Spectra, best fit model and residuals of the nucleus of M81 for the edge model (left column) and the gaussian model (right column). **Top**: PSPC; **Middle**: SAX/LECS; **Bottom**: *Chandra* -T

Table 3. BEST FIT MODEL TO THE CIRCUMNUCLEAR GALACTIC EMISSION FROM *Chandra*

Component	Parameters	Point sources Spectrum **a**	Diffuse emission Spectrum **b**
	N_H (10^{20} cm^{-2})	$4.1^{+0.4}$	$4.1^{+0.4}$
Power-law	Γ	$1.74^{+0.05}_{-0.04}$	$1.74^{+0.05}_{-0.04}$
	Flux (erg sec^{-1}cm^{-2})	6.5×10^{-13}	4.6×10^{-13}
MCBB	kT (keV)	$0.083^{+0.003}_{-0.006}$	···
	Flux (erg sec^{-1}cm^{-2})	8.9×10^{-14}	···
Gaussian	E (keV)	$0.86^{+0.03}_{-0.04}$	···
	σ (keV)	0.15 ± 0.03	···
	Flux (erg sec^{-1}cm^{-2})	7.0×10^{-14}	···
Raymond-Smith	kT (keV)	···	0.273 ± 0.011
	Flux (erg sec^{-1}cm^{-2})	···	2.3×10^{-13}
	χ^2/ν	256/197	169/126

Note. — The NH is constrained to be not less than the Galactic line-of-sight value (4.1×10^{20} cm^{-2}). All fluxes are calculated in the 0.5-2.5 keV band and corrected for best fit NH

Table 4. BEST FIT MODELS FOR THE NUCLEAR EMISSION

Model	Parameters	PSPC	SAX	*Chandra*
Power-law	N_H (10^{20} cm^{-2})	$6.8^{+0.5}_{-0.4}$	$8.3^{+1.8}_{-1.6}$	24 ± 4
	Γ	2.43 ± 0.05	$1.84^{+0.07}_{-0.06}$	2.3 ± 0.2
	Power law flux	9.8×10^{-12}	1.9×10^{-11}	...
	χ^2/ν	30.9/28	79/65	187/130
Power law	N_H (10^{20} cm^{-2})	$6.3^{+0.6}_{-0.5}$	8.0 ± 2.0	32^{+18}_{-8}
+ Raymond	Γ	$2.38^{+0.9}_{-0.7}$	$1.78^{+0.08}_{-0.09}$	$2.2^{+0.3}_{-0.2}$
	Power law flux	9.3×10^{-12}	2.0×10^{-11}	...
	kT (keV)	$0.8^{+0.5}_{-0.3}$	$0.9^{+0.5}_{-0.7}$	$0.21^{+0.06}_{-0.05}$
	Raymond flux	3.1×10^{-13}	8.4×10^{-13}	...
	χ^2/ν	21.4/26	74.5/63	161/128
Power law	N_H (10^{20} cm^{-2})	$5.1^{+1.1}_{-1.5}$	12^{+10}_{-5}	36^{+30}_{-20}
+ MCBB	Γ	$2.1^{+0.3}_{-0.8}$	$1.7^{+0.2}_{-0.3}$	2.0 ± 0.3
	Power law flux	9.1×10^{-12}	1.9×10^{-11}	...
	kT (keV)	0.27 ± 0.03	$0.24^{+0.11}_{-0.08}$	0.17 ± 0.05
	$R_{in} \times \sqrt{cos\theta}$ (km)	$2.3^{+1.3}_{-1.0} \times 10^3$	$5^{+49}_{-2} \times 10^3$	...
	MCBB flux	8.6×10^{-13}	4.9×10^{-12}	...
	χ^2/ν	18.7/26	68.3/63	162/128
Power law	N_H (10^{20} cm^{-2})	$7.1^{+0.7}_{-1.2}$	$1.3^{+3.0}_{-1.3}$	< 2.7
* edge	Γ	2.57 ± 0.10	1.77 ± 0.06	$2.11^{+0.16}_{-0.14}$
	Flux	1.0×10^{-11}	2.0×10^{-11}	...
	E (keV)	$0.41^{+0.08}_{-0.14}$	$0.22^{+0.03}_{-0.06}$	$0.29^{+0.03}_{-0.16}$
	τ	$0.4^{+1.2}_{-0.2}$	6^{+8}_{-3}	> 6
	χ^2/ν	18.1/26	69.8/63	158/128
Power law	N_H (10^{20} cm^{-2})	6.8 ± 0.5	5^{+3}_{-5}	1^{+6}_{-1}
+ gaussian	Γ	$2.48^{+0.11}_{-0.05}$	$1.77^{+0.09}_{-0.11}$	$1.86^{+0.19}_{-0.12}$
	Power law flux	9.9×10^{-12}	2.0×10^{-11}	...
	E (keV)	$0.52^{+0.06}_{-0.20}$	$0.29^{+0.07}_{-0.29}$	$0.35^{+0.06}_{-0.34}$
	σ (keV)	< 0.29	$0.09^{+0.14}_{-0.05}$	$0.09^{+0.11}_{-0.04}$
	Eq. width (eV)	-20.6	-255	-318
	Flux taken by Gauss.	-3.0×10^{-13}	-1.7×10^{-13}	...
	χ^2/ν	17.8/25	70.2/62	104/127

Note. — The model derived from *Chandra* data for the galactic emission (Table 3) is also included in the fit as a fixed component for SAX and PSPC data. Quoted N_H are in excess of the Galactic line of sight value (4.1×10^{20} cm^{-2}). Fluxes for each model component (in units of erg sec^{-1}cm^{-2}) are calculated in the 0.5-2.4 keV range and are corrected for cold absorption. Quoted errors ar at 90% confidence level for one interesting parameter.

5. DISCUSSION

5.1. Variability.

We have detected flux variability on various time scales, from a few hours to years (Section 3). At least 12 of the light curves of the individual PSPC and HRI observations (binned on the GTIs) show variability at a high confidence level, on timescales of ~ 1 day. Since the sampling of the ROSAT data is sparse, searches for periodic signals or characteristic timescales are unreliable. The variability appears to be characterized mainly by three fast X-ray shots, rising and decaying in 2 to 20 days (observations 1, 3, 10) followed by a slow rise over the next few years, and then becoming irregular after 1997.

5.1.1. Short timescales.

M81 is part of a sample of LLAGN that are observed to be less variable, on timescales less than a day, than "normal" AGN. Four ASCA observations of M81 show that its behaviour is consistent with that of the other LLAGN in the sample. Ptak et al. (1998) compared the amplitude of the variability (through the "excess variance" calculation, see Nandra et al. 1996) of a sample of LLAGN with that of Seyfert galaxies examined in Nandra et al. (1996) and found that while the latter show a significant anti-correlation between the X-ray luminosity and the excess variance, the LLAGNs are well outside of this trend, as their excess variance is apparently independent of luminosity and indicative of a much smaller amplitude of variation. Ptak et al. (1998) suggested that this difference in the variability trend of the Seyfert galaxies and LLAGN could be due to the presence of an ADAF in the LLAGNs. In an ADAF the X-ray radiation comes from a region (the ADAF corona) that is much larger than the X-ray emitting region of disks in Seyfert nuclei, leading to small amplitude variations on longer time scales. Pellegrini et al. (2000) suggested that the X-ray spectrum of the nucleus of M81 could indeed be the signature of an ADAF at work, in an intermediate accretion rate regime, where the main emitting process is inverse Compton scattering rather than bremsstrahlung.

However, using a sample of six quasars plus the Nandra et al. 1996 sample of AGN, Fiore et al. (1998) showed that the excess variance σ^2_{RMS} is instead correlated with the slope of the spectrum, rather than the luminosity, and that flatter spectrum sources tend to be less variable on a 2-20 day timescale than steeper spectrum sources. M81 has a relatively flat spectrum and the excess variance from three ASCA observations (Ptak et al. 1998) agrees with the Fiore et al. (1998) σ^2_{RMS} vs. Γ correlation for timescales of 1 day or less. However, looking at the whole set of available observations, we find that 2 to 20 days is the timescale

of the two flare events, and this suggests that M81 could lie well above the Fiore et al. (1998) correlation. The full M81 dataset also does not fit the Ptak et al. (1998) σ^2_{RMS} vs. L and instead shows an amplitude variability consistent with normal, non ADAF, AGN. A similar behaviour is observed by Gliozzi, Sambruna & Brandt (2003) in NGC 4261, a giant elliptical radio galaxy with a LINER nucleus, that hosts a low luminosity AGN: on the base of XMM-Newton light-curve and hardness ratio evolution, the authors conclude that the X-ray variability is related to the accretion flow.

If the observed flares are due to a dynamical instability, so that their timescales correspond to the Keplerian period, we can estimate the radius R at which the flare is produced, using the time interval between the flare and the closest observation with lower flux (1P-2P = 2d, 2P-3P = 20d) . The Keplerian time is:

$$t_K = \left(\frac{R^3}{GM}\right)^{1/2} = 1.4 \times 10^{-5} \sqrt{\frac{R}{R_S}^3}\, M/M_\odot \qquad (1)$$

where G is the gravitational constant, R/R_S is the radius in units of Schwartzchild radii, M is the central mass and $M_\odot$ is the solar mass. Using the estimated limits of $3 \times 10^6 M_\odot < M < 6 \times 10^7 M_\odot$ for the mass of the nuclear black hole in M81 (Ho, Filippenko, Sargent 1996; Bower et al. 2000) we get $35 < R/R_S < 260$ for the 2d flare and $160 < R/R_S < 1200$ for the 20d flare.

5.1.2. Long timescales.

The regularity of the rise from late 1994 to 1997 is broken by some irregular fluctuations in the last 3 years of observations (1997-2000, Figure 1). The slow increasing trend could be interpreted as a steady increment of the accretion rate. In the case of M81 this increment must be small enough not to modify the emitted spectrum significantly. Assuming for the central black hole a mass of $3\times10^6 M_\odot - 7\times10^7 M_\odot$ (Ho, Filippenko, Sargent 1996; Bower et al. 2000), we get an Eddington luminosity of $4.5\times10^{44} - 9\times10^{45}$ erg/s. If 10% of the luminosity is emitted in X-rays (e.g. Elvis et al. 1994) and produced by accretion with efficiency $\eta = 0.06$ (Frank, King & Raine 1992), we would have $L_{Bol}/L_{Edd} = 1.1 \times 10^{-3} - 2.2 \times 10^{-2}$ and an accretion rate $\dot{M} = L_{Bol}/(\eta c^2) = 3 \times 10^{-5} M_\odot/yr$. If the change in luminosity during the 1994-1997 steady rise is entirely due to a change in the accretion rate, this would mean that $\dot{M}$ has doubled during the same period.

If the nucleus of M81 hosts an ADAF (e.g. Narayan & Yi 1994), as suggested by Pellegrini et al. (2000) based on the lack of reflection features and of the thermal blue bump, the inferred accretion rate would locate it between the quiescent and the low state regime,

characterised by $\dot{M}/\dot{M}_{EDD} \lesssim 0.08$ (Esin, Mc Clintock and Narayan 1997).

5.2. The spectrum.

As described in Section 1, there is a general agreement on the description of the 2.0-10.0 keV continuum of the nucleus of M81 (a power law with $\Gamma \simeq 1.85$: Ishisaki et al. 1996; Pellegrini et al. 2000), while some variety of results still exists with regard to the soft X-ray emission. Using *Chandra* data we were able to estimate the contribution to the soft emission due to circum-nuclear point sources and hot ISM, and therefore to derive cleaner nuclear spectra from the larger beams of the ROSAT/PSPC and SAX/LECS.

5.2.1. The circum-nuclear emission.

The integrated spectrum of the point sources (**a**) is consistent with a power-law plus a soft component, best-fitted with a MCBB with kT=0.082 ± 0.006 keV and a large gaussian-like feature at $0.84^{+0.04}_{-0.05}$ keV (F-test probability for the addition of this component lower than 10^{-9}). The power-law is consistent with the typical spectra of low mass X-ray binaries (LMXB). The presence of a thermal component due to accretion from a disk is also common in LMXB, but we would expect a much higher temperature ($\sim$ 1 keV, e.g. Frank, King & Raine 1992). Together with the presence of the Gaussian feature, this suggest that the the soft spectrum could be quite complex, as it includes many sources that may have very different spectra. However, an accurate study of the point-like sources spectrum is beyond the aim of this work. For more details on this topic see Swartz et al. (2003). The spectrum of the diffuse emission (**b**) contains a power-law that is very similar to spectrum **a** and could be due to unresolved compact sources. It also includes a significant contribution from a Raymond-Smith spctrum that most probably comes from hot ISM. Borozdin & Priedhorsky (2000) find a very similar spectrum (with the same ratio of 0.5 between the power-law and the thermal component fluxes) when analysing the ROSAT/PSPC spectrum of the unresolved emission in the central region (less than 8') of M31. Comparing this spectrum with that of the LMXBs in the same region, they conclude that the thermal spectrum is most probably produced by truly diffuse emission from interstellar gas.

In their analysis of an XMM/RGS spectrum of the nucleus of M81 extracted from a strip 52" to 75" wide in the cross dispersion direction, Page et al. (2003) report the presence of three different thermal components, with temperature 0.18, 0.64 and 1.7 keV. They conclude that the first two are consistent with hot ISM produced by supernova remnants, while the

third (and part of the second) could be produced by LMXB. They measure a flux of 8.7×10^{-13} erg $sec^{-1}cm^{-2}$ for the sum of these components. This value is roughly half the flux of spectrum **c** (the sum of spectra **a** and **b**), but it is not easily comparable with our value, because of the different conditions of extraction (imaging in ACIS vs. dispersed spectrum in RGS).

In both **a** and **b** spectra the NH is consistent with the Galactic value along the line of sight. This implies that the excess of cold absorption seen in the nuclear spectra collected with the wide beam instruments (see below) is intrinsic to the nucleus.

5.2.2. The nuclear emission.

In the PSPC, BeppoSAX and *Chandra* -T spectra we detect an excess of NH with respect to the Galactic line of sight value (4.1×10^{20} cm^{-2}). This excess ranges from 2 to 32×10^{20} cm^{-2}, depending on the model and instrument. This is in agreement with the excess of 2 to 44×10^{20} cm^{-2} found by other instruments (*Einstein*, Fabbiano 1988, ASCA, Ishisaki et al. 1996; BeppoSAX, Pellegrini et al. 2000, this work; PSPC, this work, Immler & Wang 2001; XMM/RGS, Page et al. 2003). The *Chandra* circumnuclear spectra are well fitted with the Galactic line of sight value, clearly showing that this excess of NH is intrinsic to the nucleus.

The spectrum is not consistent with a single power-law in any of the data sets, all of which show an absorption-like feature at $\lesssim 0.4$ keV, superimposed on a power-law fit. A Power-law + MCBB model gives acceptable results, with similar values in the ROSAT, BeppoSAX and *Chandra* data. The observed temperature is hotter than that expected for a Schwartzchild black hole of the mass of M81 (0.007-0.014 keV) but is consistent with that expected for a Kerr black hole (0.39-0.83 keV). However, the normalization of the model implies an inner disk radius of $< 5 \times 10^4$ km if seen face on. This is smaller than the Schwartzchild radius of $(4.5 - 70) \times 10^6$ km for a $(3 - 60) \times 10^6 M_\odot$ black hole as in M81. A consistent Power-law+MCBB model requires the disk to be almost edge-on ($\theta \sim 90^\circ$) as well as needing a Kerr black hole. Makishima et al. (2000) made the same suggestion in the analogous case of ULXs in galaxies.

Alternatively, the feature can be fitted with an absorption edge. The optical depth of the edge is variable, and is not seen in all of the ROSAT data, but its presence and depth are not correlated with the flux. Also, the observed edge may change energy between the three instruments: we find an energy of $0.41^{+0.08}_{-0.14}$ keV in the PSPC, $0.22^{+0.03}_{-0.06}$ in BeppoSAX and $0.29^{+0.03}_{-0.16}$ in *Chandra* . These measurements are consistent at the 95% confidence level with the neutral C K edge at 0.284 keV. Alternatively, we may be detecting either different

spectral features or a single feature found at different redshifts in different observations. The energy of the PSPC feature is consistent with the CV edge at 0.39 keV and could be produced by an ionized gas in front of the nuclear source.

If the feature seen in BeppoSAX and *Chandra* is produced by the same ion, this would require the gas to be substantially redshifted ($z = 0.34 \pm 0.09$ in *Chandra* -T and $z = 0.8 \pm 0.4$ in BeppoSAX). However, once large redshift are allowed, the PSPC may be seeing moving matter too, so we cannot exclude that the edge is produced by other elements (e.g. highly redshifted OK edge or OVII, or mildly ionized Fe, i.e from FeIX at 0.23 keV to FeXIV at 0.39 keV). In any case this model suggests that the three instruments are seeing a dynamically variable system of clouds and that in the more recent observations the clouds may be accelerating toward the nucleus. Outflow velocities of 0.1-0.3 c have been reported in several quasars for the FeK resonant absorption line (Chartas, Brandt & Gallagher 2003; Reeves, O'Brien & Ward 2003). All of these are high luminosity objects that are probably radiating at or above their Eddington limit (King & Pounds 2003), while M81 is radiating at 0.001-0.02 L_{Edd}.

A third possibility to fit the absorption features is a gaussian absorption line. This model yields by far the best fit to the *Chandra* data. The line energy is consistent either with the CV Kα line at 0.308 keV or with the CVI Kα line at 0.367 in all three instruments, but again the lack of any feature that could be associated with O makes this interpretation doubtful. The OVII line at 0.57 keV would be consistent with the best fit energy in the PSPC, but it would require a significant redshift to explain the feature in the other instruments (z$\sim$ 0.9 in BeppoSAX and z$\sim$ 0.6 in *Chandra*), implying a very dynamic evolution. In either case, however, the observed equivalent width (20 eV in the PSPC, 255 eV in SAX/LECS and 318 eV in *Chandra* /ACIS) would require equivalent hydrogen absorbing columns larger than 10^{22} cm^{-2} (Nicastro, Fiore & Matt 1999) and deep absorption edges for the corresponding ions (OVII at 0.74 keV, CV at 0.39 keV and CVI at 0.49 keV). The lack of these features seems to rule out this interpretation.

The main problem with the interpretation of the feature as a C edge (either neutral or ionized) is that there is no evidence of the corresponding O K edge or any other of the edges, expected between 0.5 and 0.8 keV, which we would expect to see in a thermal gas with solar composition. The depth of the edge would then require an over-abundance of C with respect to O by a factor of 10 or more. If the O were depleted onto large dust grains, the O edge could be substantially suppressed. Gaskell et al. (2003) argue that large dust grains are common in AGN. If the number ratio of C/O is above 1, the dust will be rich in oxides, with almost non-existent carbon grains, leaving an overabundance of atomic C in the gas phase (Whittet 2003). Elvis, Marengo & Karovska (2002) suggest that the formation

of dust could be triggered by the free expansion of quasar broad emission line clouds in an outflowing wind.

The strong flux below the absorption features in both the edge and gaussian models strongly suggest the presence of warm gas ($\sim 10^6$K). This gas would be in addition to the more highly ionized gas inferred by Pellegrini et al. (2000) from the presence of highly ionized Fe features (the emission line at 6.7 keV and the absorption edge at 8.6 keV). Dusty warm absorbers have previously been suggested in other AGN (Komossa & Bade 1998; Komossa & Breitschwerdt 2000).

6. Conclusion

We have analyzed a large set of observations of the nucleus of M81, including ROSAT, ASCA, BeppoSAX and *Chandra* observations, in order to study the spectrum and variability of this bright source.

The 20 yr coverage of the nucleus of M81, with different X-ray observatories (EXOSAT, *Einstein*, ROSAT, BeppoSAX, *Chandra* , XMM-Newton) shows variability of this source on different timescales. In particular, a steady increase of the nuclear luminosity is suggested by the frequent coverage between years 1990 and 2000, interrupted by shorter flares lasting from 2 to 20 days. Also, flickering on timescales < 1 day is visible in the ROSAT data.

The steady increase of the luminosity can be interpreted as due to a change in the accretion rate onto the central black hole from the low luminosity (PSPC) to the high luminosity (*Chandra*) observations. The 2-20 days timescale of the two major flares (observations 1P and 3P) suggest dynamical instabilities occurring at between 35 to 1200 R_S.

Analysis of the ROSAT/PSPC spectra suggests spectral variability, which can be understood with the variability of a negative residual at energies below 1 keV, relative to the best fit power-law model. This feature is confirmed by an independent analysis of BeppoSAX and *Chandra* -T spectra. Spectral analysis with a variety of models (and including the best fit estimate of the circum-nuclear emission from *Chandra*), suggests that the soft spectra can be interpreted either as thermal emission from an highly edge-on accretion disk feeding a Kerr black hole or, even better, as the absorption by warm, Oxygen-depleted, gas in front of the nucleus. In the absorber case, the gas may be either highly ionized, and in which case it must be subject to strong dynamics, or, more likely, low ionization low velocity gas. A physically plausible model to explain the lack of oxygen features is that large O-rich dust grains have been formed out of the absorbing gas.

We aknowledge S. Dyson for running the original GALPIPE data reduction for M81. This research has made use of the High Energy Astrophysics Science Archive Research Center (HEASARC), provided by NASA's Goddard Space Flight Center. This work was supported by MIUR and by NASA contract NAS 8-39073 (CXC).

REFERENCES

Arnaud, K. A., George, I. M., Tennant, A. F. 1992, Legacy, 2, 65

Barr, P., Giommi, P., Wamsteker, W., Gilmozzi, R., Mushotzky, R. F. 1985, BAAS, 17, 608

Bietenholz, M.F. et al. 1996, ApJ, 457, 604

Boese, F.G. 2000, A&AS, 141, 507

Borozdin, K.N., & Priedhorsky, W.C., 2000, ApJ, 542, L13

Bower et al. 2000, BAAS, 197, 92.03

Chartas G., Brandt W.N., Gallagher S.C., 2003, astro-ph/0306125

Conover, W.J. 1971, *Practical Nonparametric Statistics*, (Wiley)

Damiani, F., Maggio, A., Micela, G., Sciortino, S 1997, ApJ, 483, 370

David, L.P. et al. 1996, The ROSAT Users Handbook, ed. U.G. Briel et al.

de Vaucouleurs G., de Vaucouleurs A., Corwin H.G., Buta R.J., Paturel G., Fouqué P., 1991, Springer-Verlag, New-York

Elvis, M., van Speybroeck, L., 1982, ApJ, 257, L51

Elvis M., Wilkes B.J., McDowell, J.C., Green R.F., Bechtold J., Willner S.P., Oey M.S., Polomski E., Cutri R., 1994, ApJS, 95, 1

Elvis M., Marengo M., Karovska M., ApJ, 567, L107

Esin, A.A., Mc Clintock, J.E, Narayan R. 1997, ApJ, 489, 865

Fabbiano, G. 1988, ApJ, 325, 544

Fiore, F., Laor, A., Elvis, M., Nicastro, F., Giallongo, E., 1998, ApJ, 503, 607

Frank, J., King, A. & Raine, D., 1992, in *Accretion Power in Astrophysics*, Cambridge University Press

Freedman W. L. et al. 1994, ApJ, 427, 628

Gaskell C.M., Goosmann R.W., Antonucci R.R.J., Whysong D., 2003, ApJ, submitted

Gliozzi M., Sambruna R.M., Brandt W.N., 2003, A&A, 408, 949

Ho, L. C., Filippenko, A. V., Sargent, W. L. W. 1996, ApJ, 462, 183

Ho, L. C., et al. 2001, ApJ, 549L, 51

Immler, S. & Wang, Q.D., 2001, ApJ, 554 202

Ishisaki Y. et al. 1996, PASJ, 48, 237

Iwasawa, K., Fabian A., & Nandra, K., 1999, MNRAS, 307, 611

Iyomoto, N. & Makishima, K. 2001, MNRAS, 321, 767

King, A. & Pounds, K. 2003, MNRAS, in press

Komossa S., Bade N., 1998, A&A, 331, L49

Komossa S., Breitschwerdt D., 1998, Ap&SS, 272, 299

La Parola, V., Peres G., Fabbiano G., Kim D. W., Bocchino F., 2001, ApJ, 556, 47

Makishima, K. et al. 2000, ApJ, 535, 632

Nandra, K., George, I.M., Mushotzky, R.F., Turner, T.J., Yaqoob, T., 1996, ApJ, 476, 70

Narayan R. & Yi I., 1994, ApJ, 428,13

Nicastro F., Fiore F., Matt G., 1999, ApJ, 517,108

Page, M.J., et al., 2003, A&A, 400, 145

Peimbert, M. & Torres-Peimbert, S. 1981, ApJ, 245, 845

Pellegrini, S., Cappi, M., Bassani, L., Malaguti, G., Palumbo, G. G. C., Persic, M. 2000, A&A, 353, 447

Petre, R., Mushotzky, R.F., Serlemitsos, P.J., Marshall, F.E., 1993, ApJ, 418, 644

Pfeffermann, E. et al. 1987, Proc. SPIE, 733 (519), 117

Ptak, A., Yaqoob, T., Mushotzky, R., Serlemitsos, P., Griffiths, R. 1998, ApJ, 501, L37

Reeves J.N., O'Brien P.T., Ward M.J., 2003, ApJ, 593, L65

Swartz D.A., Ghosh K.K., McCollough M.L., Pannuti T.G., Tennant A.F., Wu K., 2003, ApJS, 144, 213

Tody, D. 1986, SPIE 627, 733

Whittet D.C.B., *Dust in the galactic environment*, Bristol: IoP, 2003

Worrall, D.M. et al. 1992, in Data analysis in Astronomy - IV

Zimmermann, H. U., Lewin, W., Predehl, P. et al. 1994, Nature, 367, 621